Doubly differential distribution of electron emission in ionization of uracil in collisions with 3.5-MeV/u bare C ions

A. N. Agnihotri,[1] S. Nandi,[1] S. Kasthurirangan,[2] A. Kumar,[3] M. E. Galassi,[4] R. D. Rivarola,[4] C. Champion,[5] and L. C. Tribedi[1,*]

[1]*Department of Nuclear and Atomic Physics, Tata Institute of Fundamental Research, Colaba, Mumbai 400005, India*

[2]*Department of Physics, Institute of Chemical Technology, Matunga, Mumbai 400019, India*

[3]*Nuclear Physics Division, Bhabha Atomic Research Centre, Trombay, Mumbai 400085, India*

[4]*Laboratorio de Colisiones Atómicas, Instituto de Física Rosario, Universidad Nacional de Rosario and Consejo Nacional de Investigaciones Científicas y Técnicas (CONICET), Avenida Pellegrini 250, 2000 Rosario, Argentina*

[5]*Université Bordeaux 1, CNRS/IN2P3 Centre d'Études Nucléaires de Bordeaux Gradignan (CENBG) Chemin du Solarium, BP120, 33175 Gradignan, France*

(Received 18 January 2012; revised manuscript received 21 April 2012; published 25 March 2013)

We report the energy and angular distribution of the electron emission from an RNA base molecule uracil in collisions with 3.5-MeV/u bare C ions. The absolute double differential cross sections (DDCS) are measured for emission energy between a few to 600 eV. The angular distributions are compared to those obtained for the O_2 molecule in the same experiment. The single differential cross sections (SDCS) are also deduced. The energy and angular distributions of the DDCS and SDCS are compared with the state-of-the-art quantum-mechanical models based on continuum distorted wave-eikonal initial state (CDW-EIS) and correct boundary first Born (CB1) approximations which use a suitable molecular wave function for uracil. The models, however, give substantial deviations from the observed energy and angular distributions of the DDCS as well as SDCS. The CDW-EIS calculations are closer to the data compared to the CB1. In the case of uracil a large difference in the forward-backward emission of electrons was observed in comparison to that in collisions with an oxygen molecule.

DOI: 10.1103/PhysRevA.87.032716 PACS number(s): 34.50.Gb

I. INTRODUCTION

Electron emission in the ionization of atoms and molecules by fast ions provides microscopic details of the underlying collision mechanisms. The continuum electron spectrum is very rich, providing a signature of soft collision, binary encounter, electron capture to continuum (ECC) cusp electrons [1] besides the Young-type electron interference. The angular distribution of the electron emission, and forward-backward angular asymmetry in particular, in ion-atom or ion-molecule collisions is sensitive to the so-called two-center effect (TCE) [2–7] and interference effect [8–10]. It has been demonstrated that the asymmetry also depends on the nature of the target potential, i.e., pure Coulombic (e.g., in atomic H) or non-Coulomb potential (in a multi-electron system) [11]. In the TCE the electron in its final state is influenced by the combined Coulomb field of two moving centers, i.e., the ionized target and the projectile. This effect mainly depends on the perturbation strength Z_p/v_p (Z_p is the atomic number, v_p the velocity) of the projectile. The electron double differential cross section (DDCS) ($\frac{d^2\sigma}{dEd\Omega}$), i.e., the differential in emission angle (θ) and ejected electron energy (E) provides an experimental signature of these mechanisms. The DDCS also gives a more stringent test for theoretical models than the single differential cross sections (SDCS), i.e., $\frac{d\sigma}{d\Omega}$ or $\frac{d\sigma}{dE}$ and total ionization cross sections (TCS). The high-resolution recoil-ion momentum spectroscopy technique, which provides the cross sections differential in the longitudinal and transverse momentum of all three particles in the final state, can also be used to provide a stringent test to various models [12–19] for different collision processes, such as ionization, electron capture, transfer ionization, and so on. In last two decades, it has been shown in several works that the shape of the DDCS spectrum is sensitive to the above-mentioned mechanisms [6,7,20–25]. The ECC cusp electrons are observed as a sharp peak at $v_e = v_p$ for the zero degree emission angle since these electrons move along with the projectile ion [2,24]. The binary encounter (BE) electrons are the elastically scattered target electrons from the moving projectile nucleus. The position of the binary encounter electron peak in the case of heavy-ion impact is given by $E_{\mathrm{BE}} = 4(m_e/M_p)E_p\cos^2(\theta)$, and velocity $v_{\mathrm{BE}} = 2v_p\cos(\theta)$, where m_e is the electron mass, M_p is the projectile mass, E_p the projectile energy, and θ the electron emission angle with respect to the incident projectile beam direction [2,24]. In the case of zero degree emission, the energy of the observed binary encounter electrons $v_{\mathrm{BE}} = 2v_p$ may be considered as produced in a 180° Rutherford scattering from the moving nucleus while viewed in the projectile frame.

For highly charged ions, the electron emission mechanism is more complicated than that for low-charge projectiles (electrons and protons). Indeed, the electrons emitted in collisions are highly influenced by the target ion and the moving projectile. Therefore the dynamics of the electron emission process cannot be described adequately without considering the effect of the moving projectile even after the collisions. The electron now moves in the combined field of the the target and the projectile ions. Such a TCE cannot be adequately described by the first-order perturbation model using the first Born (B1) approximation, which is essentially a single center model. It is now known that even for fast ions on simple atomic targets [4,22,23,26], the B1 approximation fails

*lokesh@tifr.res.in; ltribedi@gmail.com

to explain the angular distributions of the ionized electrons, in particular the forward enhancement. However, such a two-center electron emission is described in a better way by the models which take into account the distortion of the electron wave function by the Coulomb field of the moving charge. The continuum distorted wave eikonal initial state (CDW-EIS) is one such model which takes into account the distortion of the electron wave functions in the initial as well as final states [3]. By and large, the electron emission cross sections, its angular distributions [4,23], forward-backward asymmetry [6,7], and postcollisional interactions for simple target atoms are well described by the CDW-EIS model. However, a stringent comparison clearly indicates the deviation of models from the experimental data even for simple targets like H [22,23], H_2 [5,26], or He [4,6,26]. Forward-backward asymmetry and its deviation from the predictions of the B1 approximation are clear indicators for the TCE, which has also been studied in detail in [4,6,7,22,23]. The CDW-EIS was updated to include the multi-electronic (mostly atomic) targets [27]. For large molecules or clusters as targets, one may expect additional complexity which arises due to the ambiguity in choosing a suitable wave function. The many-body effect as well as the postcollisional interaction may also influence the electron spectrum.

It will, therefore, be of interest to investigate the mechanisms of electron emission from large molecules and to explore any observable difference with simple atoms and small molecules. Here we study the electron DDCS for fast bare carbon-ion impact ionization of an RNA base molecule uracil ($C_4H_4N_2O_2$, $m = 112$ amu). In some cases the DDCS results for O_2 [28], measured in the same experiment, are also used for comparison. Besides the inherent interest for atomic collisions, the study of electron emission from uracil is very important to provide a benchmark study of radiation damage of DNA or RNA base molecules. Indeed, for modeling the radio-induced damages for biological cells under heavy-ion impact, further *ab initio* theoretical calculations and experimental data are crucial. Such data are especially relevant in the case of C-ion projectiles which are commonly used for high-energy hadron therapy. In case of hadron therapy the ions lose energy on their way and finally come to rest. The energy loss of the ions in such processes is not uniform and the maximum energy loss occurs in a certain energy range which is called the Bragg peak region. For carbon projectile ions with ∼GeV energy, the Bragg peak energy (∼1 MeV/u) lies close to the energy studied in this work, which makes it relevant for model calculations.

The measurements on molecules of biological interest, so far, are mostly limited to the total ionization cross section (TCS) [29–34] particularly for heavy ions as projectiles. These studies along with similar other recent investigations of charge particle interaction with large biomolecules, water molecules, and fullerenes [35–42] have created a broad data base. The TCS, however, cannot give the microscopic details, such as the energy and angular distribution of the electrons emitted. The lowest-energy electrons (even below the ionization-threshold energy) are shown to be primarily responsible for the damage of biological cells [43]. In collisions with ions, a large number of low-energy electrons are produced with various energies along the ion tracks inside a body [44,45] which can cause large-scale damage. Therefore, it is important to know, with the highest degree of precision, the energy as well as the angular distributions of such low-energy electrons. So far, the electron DDCS investigations, for DNA and RNA base molecules, have been reported for a few cases [46–48] which are mainly limited to proton projectiles. In addition, the DDCS measurements on large biomolecules, in collisions with highly charged heavy ions, such as C^{6+}, have not been addressed. As already mentioned, the collisions involving such heavy ions are more complicated than those for protons or electrons as projectiles and therefore need to be investigated.

II. THEORETICAL MODELS

On the theoretical side, a model combining the classical trajectory Monte Carlo (CTMC) approach with a classical overbarrier (COB) criterion was recently employed to analyze single and multiple ionizing processes induced by the impact of fast H^+, He^{2+}, and C^{6+} ions on RNA and DNA bases in terms of the total cross sections [49,50]. The quantum-mechanical approaches developed within the first-order Born approximation with correct boundary conditions (CB1) and the CDW-EIS calculations were recently proposed to provide the DDCS, SDCS, and TCS for the proton impact on DNA components [51,52]. At this stage, let us mention that besides the ionization modeling, which is radically different within the classical and the quantum approaches, the description of the impacted biological targets are also hugely different. Indeed, in the classical approach [49,50] it is simply reduced to the knowledge of the ionization energies of the different molecular subshells of the targets, while in the quantum approaches, a complete description of the molecular wave functions in terms of the linear combinations of atomic orbitals (LCAO) is needed. Ionization orbital energies were calculated with the GAUSSIAN 09 software at the restricted Hartree-Fock (RHF)/3-21G level of theory [53]. Besides that, the complete neglect of differential overlap (CNDO) approximation, similar to Senger *et al.* [54], was used to calculate the total cross sections. The essential steps for both models are described in [34]. In both models the screening produced by the electrons remaining in the molecule on the dynamical evolution of the ionized one is only roughly taken into account [55], especially considering that the influence of the geometry of the target is neglected in the CNDO calculations.

III. EXPERIMENTAL DETAILS

The experimental setup consists of a scattering chamber housing an electrostatic hemispherical analyzer setup with a channel electron multiplier detector [56]. The energy resolution of the spectrometer was about 6% of the electron energy. The gaseous target of uracil was prepared by heating the uracil powder (99% pure, Sigma-Aldrich) in an oven. The oven assembly consists of a cooling jacket, a quartz crystal thickness monitor, and an XYZ manipulator. The uracil was heated up to 160 °C to obtain enough vapor density in the interaction region. The molecules effuse through a nozzle of a diameter of 1 mm. Maintaining a uniform flow of molecules throughout the experiments was a crucial and challenging task. To ensure this, the oven temperature was raised very

slowly and a quartz crystal thickness monitor (INFICON SQM 160 Multi-Film Rate and thickness monitor) was suitably mounted to monitor the flow of the molecules throughout the experiment. The thickness monitor contains a Cr/Au 6 MHZ crystal on which the uracil layer is deposited. The monitor shows the thickness of the deposited molecule layer (kÅ) with time and also the rate of deposition. The thickness reading was noted at regular intervals (∼5 min) throughout the experiment and the rate of deposition was monitored. The variation of the deposition rate with time, if at all, was very smooth and was found to vary by about 5–10% over a long period, i.e., in about 10 h. The vacuum in the chamber was better than 1×10^{-7} Torr. Care was taken to minimize stray electric and magnetic fields to detect the lowest-energy electrons. The experiment was carried out using 3.5-MeV/u bare C ions obtained from the 14 MV Pelletron accelerator at the Tata Institute of Fundamental Research (TIFR), Mumbai. After collimation the ion beam was crossed with the gaseous target of uracil in the scattering chamber. Electron yields over the energy range between 6 and 600 eV (i.e., for v_e between 1 and 7 a.u.) and in an angular range of 30°–135° were measured. In addition, electron DDCS measurements were also carried out for the O_2 molecule to compare with the uracil data. For this experiment a static gas pressure was used in a flooded chamber. The typical pressure used was in the range of 0.10 to 0.20 mTorr.

IV. RESULTS AND DISCUSSIONS

Figure 1 displays the typical electron DDCS spectrum for uracil at various angles along with CDW-EIS and CB1 model calculations. The energy range covers the low-energy ejected electrons emitted in soft collisions, i.e., relatively large impact parameter collisions. The spectrum extends to higher energies which include the KLL-Auger electrons from the K-shell ionization of the atoms present in the uracil molecule, which mostly arises from low-impact parameter collisions. The three KLL-Auger peaks in the higher-energy part of the DDCS spectrum correspond to C, N, and O appearing at about 240, 355, and 480 eV, respectively [shown in Fig. 1(a)]. At a given angle the electron spectra were taken with and without target (i.e., background) and the background was subtracted from the data to obtain the DDCS. The O_2 DDCS measurements [28] were performed in a static gas condition and included the KLL O-Auger peak region. The O-Auger line was used for the absolute normalization of the cross sections of uracil. Here the assumption is that the inner shell ionization (total Auger cross sections) for O is the same in the case of O_2 and uracil. The detail normalization procedure as well as the error estimation is given in the Appendix.

A. Electron DDCS: Emitted electron energy dependence

The absolute DDCS exhibit a rapid decrease (Fig. 1) with ejected electron energy, indicating the dominant contribution of the low-energy part in the electron spectrum. For example, we show the spectrum for eight different angles in Fig. 1. In the case of the forward angles, the DDCS falls from 10^{-17} cm^2/eV sr to 3×10^{-20} cm^2/eV sr, i.e., by about three orders of magnitude over a range of 600 eV. A similar fall is also noticed for

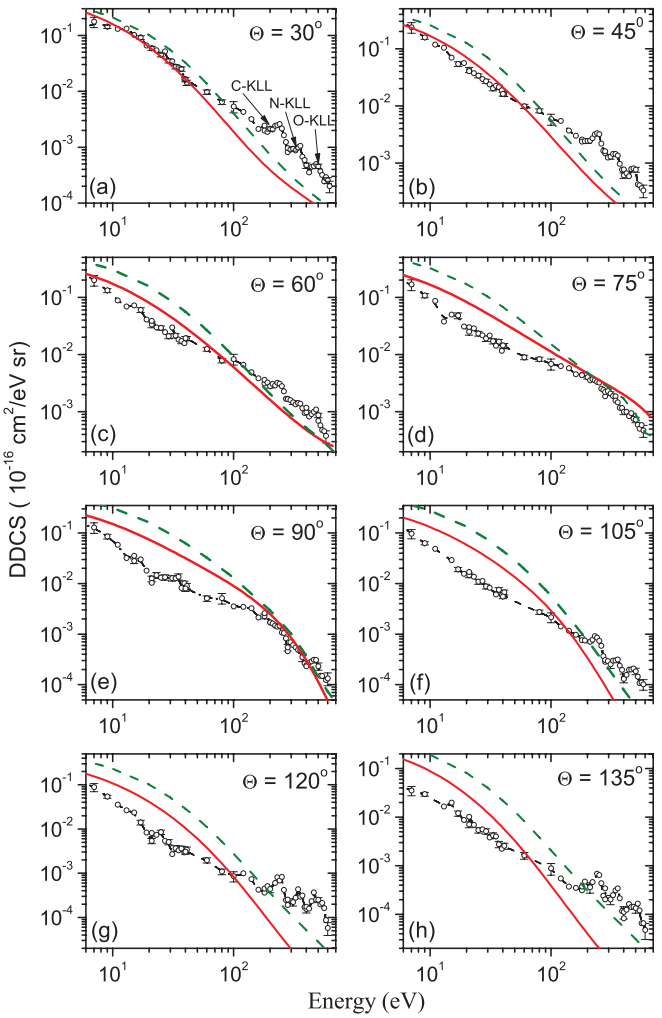

FIG. 1. (Color online) DDCS spectra of uracil in collision with 3.5-MeV/u C^{6+} ions. The solid and dashed lines are for CDW-EIS and the CB1 models, respectively.

backward angles. The CDW-EIS model is in good agreement with the experiments at 30°, but deviates with increasing scattering angle. For scattering angles larger than 30°, the absolute values predicted by the CDW-EIS model are much higher compared to the experimental data, especially below 100 eV. However, the sharp fall is qualitatively reproduced except for the backward angles. A close look into the data reveals several discrepancies. For example, the best agreement is found with the CDW-EIS model only for extreme forward angles, i.e., 30° and 45°. Even for these two angles (and also for 60°) the calculation crosses the data at ∼100 eV. For the angles 75° and 90°, over the entire energy range, the models predict higher DDCS than the data except for the higher-energy part. It may be noted that the models shown here do not include the KLL-Auger electron contribution in the spectrum. The DDCS spectrum shows an oscillatory structure overriding on the steep fall. The broad maximum at around 200 eV for 75° and 90° cannot be explained by a simple BE. For example, the expected BE peak energy will be about 510 eV for 75°. In the case of backward angles, the agreement with the DDCS data is even worse. The CDW-EIS overestimates the low-energy data (i.e., below 100 eV) by a large factor (i.e., about 3–4) and

underestimates the high-energy data by a similar large factor. Therefore, the shape or the qualitative behavior is also not so well reproduced for most of the angles. The CB1 calculation remains parallel to the CDW-EIS values almost for all the angles and predicts substantially higher values. In Fig. 1, the total error, which includes the error propagated from the normalization procedure and statistical error, is shown at three data points, i.e., in the low- (7 eV), middle- (100 eV), and high-energy regions (∼600 eV) in each panel. For the rest of the data points we show only the statistical error. The detail estimation of errors is discussed in the Appendix.

B. Electron DDCS: Fraction of low-energy electrons

As mentioned above, a large number of low-energy electrons with certain energy distribution are produced in soft collisions between the swift ions and the molecules along the ion track [44,45], which can cause further damage to the biological cells around it. To estimate the relative contribution of the low-energy electrons we have derived the ratio of the low-energy electron yield obtained by integrating the DDCS up to 40 eV (i.e., partial $d\sigma/d\Omega$ up to 40 eV) to the total yield (i.e., $d\sigma/d\Omega$) for each angle. For this purpose the cutoff energy (i.e., 40 eV) was chosen somewhat arbitrarily, but keeping in mind that most of the dissociative attachment of the low-energy electrons to the molecules [43] and the above-threshold ionization contribute roughly below this energy. The relative yields of the low-energy electrons are found to be varying between 68% to 85% with a dip at 75°, which is in approximate agreement with the model prediction. The fraction has a relatively low uncertainty, i.e., about 5–10% since it is free from normalization error. This fraction (or the overall energy distribution itself) may be used as an input for modeling the ion-induced cellular damage.

C. Electron DDCS: Angular distributions

Figure 2 shows the typical angular distributions of ejected electrons for few electron energies (i.e., for 21, 40, 100, and 180 eV). The angular distributions indicate that the electrons are preferably emitted in the forward direction. The observed DDCS for 21 eV [Fig. 2(a)] falls steadily with increasing angle, which is in contrast to the models which predict a broad peak around 80°. Only at the forward angle does the CDW-EIS agree with the data. The deviation increases gradually with the angle and for the backward-most angle studied here, the theory overestimates the data by a factor of 3 to 4. At slightly higher energy (e.g., 40 eV, the data start showing a broad peak around 60° which moves to 80° for higher-energy electrons (e.g., 180 eV) [see Figs. 2(b) to 2(d)]. Both the models show a broad peak at around 80° in each case. However, the CDW-EIS approaches the measured distributions at higher energies. For 100 eV data, the CDW-EIS provides a better agreement, whereas for 180 eV the agreement is limited to the middle angles, i.e., about 60° to 105°. The large deviations at the forward and backward angles are obvious. The CB1 calculation provides a better agreement with all the backward angles for the 180-eV data. It may also be noticed that for low energies (e.g., 21 and 40 eV) the forward emission is about six to seven times larger than that for the backward angles for

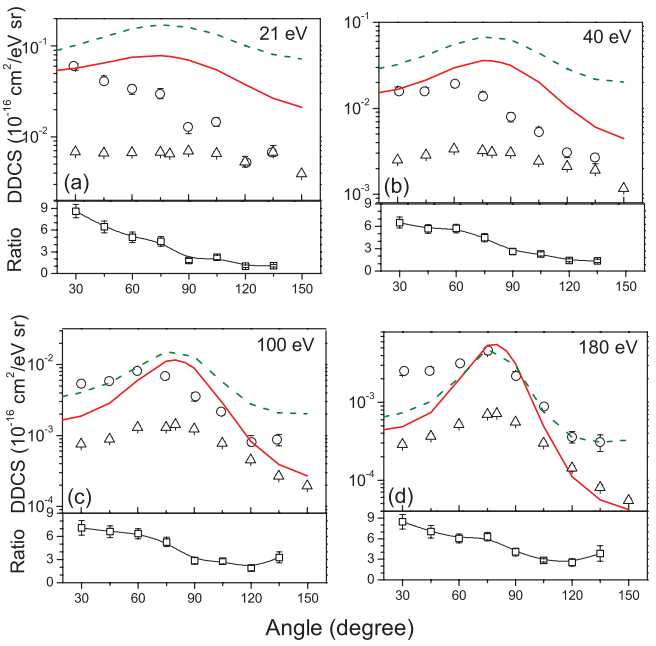

FIG. 2. (Color online) Angular distribution of ejected electrons of different energies from uracil (circles) and O_2 (triangles) targets. The solid and dashed lines are for CDW-EIS and the CB1 models, respectively, for uracil. The ratios of DDCS of uracil to O_2 are shown below each panel.

uracil. However, the models do not explain the unusually large forward enhancement. One can also note that the distributions for 21, 40, and 100 eV are peaked at slightly lower angles than the predictions of the models. It may, therefore, be suggested that the mechanism responsible for electron emission in the case of uracil is probably more complicated than for simple ion-molecule collisions.

To compare it to the expected results for collisions with a small molecule, we have plotted the distributions obtained for O_2 in the same experiment [see the triangles in Figs. 2(a) to 2(d)]. In the case of 21 eV the DDCS for uracil at the forward angle is almost one order of magnitude higher than that for the large backward angle. This behavior is quite different than that for O_2 for which the distribution is rather flat at 21 eV [the triangles in Fig. 2(a)]. Similarly, for the 40-eV energy the forward enhancement (in the case of O_2) is only about 1.3 where the cross sections vary from 2.5×10^{-19} cm^2/eV sr to 1.9×10^{-19} cm^2/eV sr in the angular range of 30° to 135°. In contrast, for the uracil molecule the forward emission is about six to seven times larger than that for the backward direction. These are better represented in Figs. 2(a) to 2(d) in which we show the ratio of DDCS for uracil to that of O_2. In each case the ratio is quite large for the forward-most angles and approaches to the value of unity for the backward angles for low energies (21 and 40 eV) and a value of about three for higher energies (100 and 180 eV). If the ionization mechanism is the same for both molecules then one would expect approximately a constant ratio, i.e., independent of the angles, but that is not the situation.

The origin of the this large forward enhancement is not very clear. A part of this can be due to the postcollision interactions (PCI). The PCI with the emitted electron has two components,

one of which arises from the projectile and another from the residual target. In the present case the projectile is the same for both collision systems and the residual targets are singly ionized molecules, i.e., O_2^+ and uracil$^+$. Therefore, the PCI do not seem to be too different from each other. The only difference is the size and the structure of the target molecule, which probably can cause such a difference. The bigger size of the molecule can cause the screening of the residual charge on the molecule, which will be different than a small atom or molecule. Such a screening on the parent molecule may act to reduce the backward scattering of the emitted electrons. It may be speculated that one has to include many-body effects, such as collective excitations or multi-electron correlations, while describing the electron emission from uracil and such effects are beyond the present theoretical models.

D. Electron SDCS: Energy and angular distribution

To understand the overall angular and energy distribution of electrons emitted in the collisions, the SDCS were plotted as a function of angle and energy. Figures 3(a) and 3(b) display the absolute electron SDCS spectra for uracil target. The angular distribution of the SDCS ($\frac{d\sigma}{d\Omega}$) deduced by integrating DDCS over the electron energy. Figure 3(b) shows the energy distribution of the SDCS, i.e., $\frac{d\sigma}{dE}$ calculated by integrating the DDCS over the emission angle. The SDCSs were then compared with the CDW-EIS and CB1 models. The CDW-EIS model matches well with the $\frac{d\sigma}{d\Omega}$ for angles up to 60°, but overestimates the experimental data for higher angles [Fig. 3(a)]. The shape of the calculated distribution also differs from the data. The measured SDCS shows a peak at a lower forward angle than that predicted by the models. The CB1 calculation remains parallel to CDW-EIS, but predicts larger values. As far as the $\frac{d\sigma}{dE}$ is concerned, the CDW-EIS model approximately reproduces the sharp fall but overestimates the experiment till 200 eV. The CB1 model predicts values higher than CDW-EIS. It can be seen that for the $\frac{d\sigma}{dE}$ the CDW-EIS does not cross the data at 100 eV, as in most of the cases for DDCS spectrum. The three Auger peaks are also visible in the SDCS spectrum [see the inset in Fig. 3(b)]. It may be noted that the models show a smoothly decreasing behavior in contrast to the structure observed in the shape of experimental SDCS spectrum.

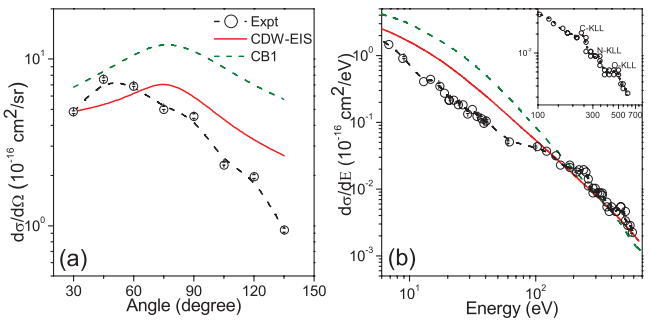

FIG. 3. (Color online) The absolute SDCS as a function of (a) angle and (b) energy of the electron emission from uracil.

V. CONCLUSION

We have measured the energy and angular distribution of low-energy electron emission from the uracil molecule in collisions with bare C ions of energy 3.5 MeV/u. The single differential distributions in terms of angle and electron energy are also deduced. The lowest-energy electrons (below 40 eV) which are mainly responsible for radiation damage are found to constitute almost 80% of the total electron emission cross section. An extensive comparison with two theoretical models is presented. The overall energy and angular distributions of the measured DDCS reveal a substantial discrepancy with both the quantum-mechanical models, i.e., CDW-EIS and the CB1. Both the SDCSs, i.e., $\frac{d\sigma}{d\Omega}$ and $\frac{d\sigma}{dE}$ show certain deviations from the the models regarding the shape and the absolute values. In general the CB1 gives a larger deviation than the CDW-EIS. The angular distributions of DDCS for uracil show certain distinct differences with those for simple ion-molecule collisions. Unusually large forward enhancement and backward depletion of the electron emission have been observed, which is in contrast to that observed for O_2.

ACKNOWLEDGMENT

The authors thank the Pelletron accelerator team for the smooth running of the machine.

APPENDIX: NORMALIZATION PROCEDURE

The absolute normalization of the uracil DDCS data was done in two steps. In the first step, the absolute values for DDCSs for the O_2 target were obtained from the first principle [56]. For this purpose the quantities like the beam intensity and target thickness were determined accurately. Several other measured quantities like spectrometer geometry including the apertures and path-length-solid-angle integral, the emission angles, and finally the resolution of the spectrometer were used along with the known detection efficiency of the channel electron multiplier (CEM). The front of the CEM was raised to 100 eV. Therefore effectively all the low-energy electrons up to 600 eV were detected with the same efficiency since the efficiency of the CEM in this energy range is constant (i.e., 0.83 as obtained from the manual of the CEM). The beam intensity was measured in an electrically isolated Faraday cup with a suitable geometry to minimize the loss of backscattered electrons. The target thickness for the static gas condition was measured from the pressure determined by a well-calibrated (MKS) Baratron pressure gauge. The background spectrum was taken with no gas in the chamber and was subtracted from the oxygen spectrum. The absolute DDCS for the O_2 target were then integrated over the O-KLL Auger peak region for each angle to provide the SDCS ($\frac{d\sigma}{d\Omega}$). After integrating the SDCS (KLL) over the angles, the absolute total Auger emission cross sections (σ_{KLL}) were then obtained.

In the second step, the relative SDCS ($\frac{d\sigma}{dE}$) spectrum in uracil ionization was plotted [Fig. 3(b)]. This spectrum which was obtained from a jet target has two parts: (i) the continuum part and (ii) the KLL-Auger peaks (C, N, O). Both (i) and (ii) thus are produced from same target thickness, jet profile, beam overlap, and are associated with the same solid angle.

The total yield (Y_{KLL}) of the oxygen KLL-Auger line was then obtained by integrating the SDCS ($\frac{d\sigma}{dE}$) spectrum [Fig. 3(b)] over the O-Auger line. A linear baseline subtraction was done by suitably choosing the points on either sides of the peak. The yield is given by, $Y_{KLL} = \sigma_{KLL} G \epsilon(E) N_p$ where G represents the target thickness convoluted with the jet-profile and path-length integrals. The number of projectile ions is denoted by N_p. Here we have assumed that the O-KLL Auger emission cross section (σ_{KLL}) is the same in the case of O_2 and the uracil molecule since it is an inner-shell ionization process. In this way the unknown quantity G was determined, which was then used to normalize the entire electron DDCS spectrum [i.e., (i) and (ii)] obtained for uracil. The error estimated in the normalization procedure is ∼20%. For most of the angles and most of the energies the statistical error varies between 15–25% giving the total error of about 25–30%. In a few cases, i.e., for extreme higher energies (i.e., around 560 eV and for a few angles the statistical error itself can be about 25–30%. In addition, a systematic error of about 10% arising from the background subtraction method cannot be ruled out.

[1] N. Stolterfoht, R. D. DuBois, and R. D. Rivaola, *Electron Emission in Heavy Ion Atom Collision* (Springer, Berlin, 1997).

[2] D. H. Lee, P. Richard, T. J. M. Zouros, J. M. Sanders, J. L. Shinpaugh, and H. Hidmi, Phys. Rev. A **41**, 4816 (1990).

[3] P. D. Fainstein, V. H. Ponce, and R. D. Rivarola, J. Phys. B: At. Mol. Opt. Phys. **24**, 3091 (1991).

[4] N. Stolterfoht, H. Platten, G. Schiwietz, D. Schneider, L. Gulyás, P. D. Fainstein, and A. Salin, Phys. Rev. A **52**, 3796 (1995).

[5] L. C. Tribedi, P. Richard, Y. D. Wang, C. D. Lin, and R. E. Olson, Phys. Rev. Lett. **77**, 3767 (1996).

[6] D. Misra, A. Kelkar, U. Kadhane, A. Kumar, Y. P. Singh, L. C. Tribedi, and P. D. Fainstein, Phys. Rev. A **75**, 052712 (2007).

[7] S. Suárez, C. Garibotti, W. Meckbach, and G. Bernardi, Phys. Rev. Lett. **70**, 418 (1993).

[8] N. Stolterfoht, B. Sulik, V. Hoffmann, B. Skogvall, J. Y. Chesnel, J. Rangama, F. Frémont, D. Hennecart, A. Cassimi, X. Husson, A. L. Landers, J. A. Tanis, M. E. Galassi, and R. D. Rivarola, Phys. Rev. Lett. **87**, 023201 (2001).

[9] D. Misra, U. Kadhane, Y. P. Singh, L. C. Tribedi, P. D. Fainstein, and P. Richard, Phys. Rev. Lett. **92**, 153201 (2004).

[10] D. Misra, A. Kelkar, U. Kadhane, A. Kumar, and L. C. Tribedi, Phys. Rev. A **74**, 060701(R) (2006).

[11] P. D. Fainstein, L. Gulyés, F. Martin, and A. Salin, Phys. Rev. A **53**, 3243 (1996).

[12] R. Moshammer, J. Ullrich, H. Kollmus, W. Schmitt, M. Unverzagt, H. Schmidt-Bocking, C. J. Wood, and R. E. Olson, Phys. Rev. A **56**, 1351 (1997).

[13] J. Ullrich, R. Moshammer, R. Dörner, O. Jagutzki, V. Mergel, H. Schmidt-Bocking, and L. Spielberger, J. Phys. B: At. Mol. Opt. Phys. **30**, 2917 (1997).

[14] M. Schulz *et al.*, Phys. Rev. Lett. **108**, 043202 (2012), and references therein.

[15] J. Titze *et al.*, Phys. Rev. Lett. **106**, 033201 (2011).

[16] M. Schulz, R. Moshammer, D. Fischer, H. Kollmus, D. H. Madison, S. Jones, and J. Ullrich, Nature (London) **422**, 48 (2003).

[17] N. V. Maydanyuk, A. Hasan, M. Foster, B. Tooke, E. Nanni, D. H. Madison, and M. Schulz, Phys. Rev. Lett. **94**, 243201 (2005).

[18] M. Schulz, Phys. Scr. **80**, 068101 (2009).

[19] M. Dürr, C. Dimopoulou, B. Najjari, A. Dorn, K. Bartschat, I. Bray, D. V. Fursa, Z. Chen, D. H. Madison, and J. Ullrich, Phys. Rev. A **77**, 032717 (2008).

[20] N. Stolterfoht, H. Platten, G. Schiwietz, D. Schneider, L. Gulyás, P. D. Fainstein, and A. Salin, Phys. Rev. A **52**, 3796 (1995).

[21] P. D. Fainstein, V. H. Ponce, and R. D. Rivarola, J. Phys. B: At. Mol. Opt. Phys. **24**, 3091 (1991).

[22] L. C. Tribedi, P. Richards, W. DeHaven, L. Gulyás, M. W. Gealy, and M. E. Rudd, J. Phys. B: At. Mol. Opt. Phys. **31**, L369 (1998).

[23] L. C. Tribedi, P. Richard, L. Gulyás, M. E. Rudd, and R. Moshammer, Phys. Rev. A **63**, 062723 (2001).

[24] T. J. M. Zouros, K. L. Wong, S. Grabbe, H. I. Hidmi, P. Richard, E. C. Montenegro, J. M. Sanders, C. Liao, S. Hagmann, and C. P. Bhalla, Phys. Rev. A **53**, 2272 (1996).

[25] L. C. Tribedi, P. Richard, Y. D. Wang, C. D. Lin, and R. E. Olson, Phys. Rev. Lett. **77**, 3767 (1996).

[26] L. C. Tribedi, P. Richard, L. Gulyás, and M. E. Rudd, Phys. Rev. A **63**, 062724 (2001).

[27] L. Gulyás, P. D. Fainstein, and A. Salin, J. Phys. B: At. Mol. Opt. Phys. **28**, 245 (1995).

[28] S. Nandi, A. N. Agnihotri, S. Kasthurirangan, A. Kumar, C. A. Tachino, R. D. Rivarola, F. Martín, and L. C. Tribedi, Phys. Rev. A **85**, 062705 (2012).

[29] J. de Vries, R. Hoekstra, R. Morgenstern, and T. Schlathölter, Phys. Scr., T **110**, 336 (2004).

[30] R. Brédy, J. Bernard, L. Chen, M. C. Buchet-Poulizac, and S. Martin, Nucl. Instr. Meth. B **261**, 114 (2007).

[31] M. Imhoff, Z. Deng, and M. A. Huels, Int. J. Mass Spec. **245**, 68 (2005).

[32] J. Bernard, R. Bredy, L. Chen, S. Martin, and B. Wei, Nucl. Instr. Meth. B **245**, 103 (2006).

[33] T. Schlathölter, F. Alvarado, S. Bari, A. Lecointre, R. Hoekstra, V. Bernigaud, B. Manil, J. Rangama, and B. Huber, Chem. Phys. Chem. **7**, 2339 (2006).

[34] A. N. Agnihotri, S. Kasthurirangan, S. Nandi, A. Kumar, M. E. Galassi, R. D. Rivarola, O. Fojón, C. Champion, J. Hanssen, H. Lekadir, P. F. Weck, and L. C. Tribedi, Phys. Rev. A **85**, 032711 (2012).

[35] H.-W. Jochims, M. Schwell, H. Baumgartel, and S. Leach, Chem. Phys. **314**, 263 (2005).

[36] M. Imhoff, Z. Deng, and M. A. Huels, Int. J. Mass Spec. **262**, 154 (2007).

[37] H. J. Lüdde, T. Spranger, M. Horbatsch, and T. Kirchner, Phys. Rev. A **80**, 060702(R) (2009).

[38] J. Tabet, S. Eden, S. Feil, H. Abdoul-Carime, B. Farizon, M. Farizon, S. Ouaskit, and T. D. Mörk, Phys. Rev. A **82**, 022703 (2010).

[39] W. Friedland, M. Dingfelder, P. Kundrát, and P. Jacob, Mutation Research **711**, 28 (2011).

[40] E. Surdutovich, G. Setzler, W. E. Kauppila, S. J. Rehse, and T. S. Stein, Phys. Rev. A **77**, 054701 (2008).
[41] A. H. Kelkar, U. Kadhane, D. Misra, L. Gulyas, and, L. C. Tribedi, Phys. Rev. A **82**, 043201 (2010).
[42] U. Kadhane, A. Kelkar, D. Misra, A. Kumar, and L. C. Tribedi, Phys. Rev. A **75**, 041201(R) (2007).
[43] B. Boudaïffa, P. Cloutier, D. Hunting, M. A. Huels, L. Sanche *et al*., Science **287**, 1658 (2000).
[44] L. Sanche, Mass Spectrom. Rev. **21**, 349 (2002).
[45] L. Sanche, Eur. Phys. J. D **35**, 367 (2005).
[46] B. Coupier, B. Farizon, M. Farizon, M. J. Gaillard, F. Gobet, N. V. de Castro Faria, G. Jalbert, S. Ouaskit, M. Carré, B. Gstir, G. Hanel, S. Denifl, L. Feketeova, P. Scheier, and T. D. Mörk, Eur. Phys. J. D **20**, 459 (2002).
[47] P. Moretto-Capelle and A. Le Padellec, Phys. Rev. A **74**, 062705 (2006).
[48] Y. Iriki, Y. Kikuchi, M. Imai, and A. Itoh, Phys. Rev. A **84**, 032704 (2011).
[49] I. Abbas, C. Champion, B. Zarour, B. Lasri, and J. Hanssen, Phys. Med. Biol. **53**, N41 (2008).
[50] H. Lekadir, I. Abbas, C. Champion, O. Fojón, R. D. Rivarola, and J. Hanssen, Phys. Rev. A **79**, 062710 (2009).
[51] C. Champion, H. Lekadir, M. E. Galassi, O. Fojón, R. D. Rivarola, and J. Hanssen, Phys. Med. Biol. **55**, 6053 (2010).
[52] M. E. Galassi, C. Champion, P. F. Weck, R. D. Rivarola, O. Fojón, and J. Hanssen, Phys. Med. Biol. **57**, 2081 (2012).
[53] M. J. Frisch *et al*., GAUSSIAN 09, Revision A.02, Gaussian, Inc., Wallingford, CT (2009).
[54] B. Senger, Z. Phys. D: At. Mol. Clusters **9**, 79 (1988).
[55] J. M. Monti, O. Fojón, J. Hanssen, and R. D. Rivarola, J. Phys. B **43**, 205203 (2010).
[56] D. Misra, K. V. Thulasiram, W. Fernandes, A. H. Kelkar, U. Kadhane, A. Kumar, Y. Singh, L. Gulyós, and L. C. Tribedi, Nucl. Instru. Meth. B **267**, 157 (2009).